A first-principles investigation of physical properties and superconductivity of NbPS

H. M. Tütüncü[1,2], Ertuğrul Karaca[2], H. Y. Uzunok[1,2], S. Bağcı[1], G. P. Srivastava[3]

[1] *Sakarya Üniversitesi, Fen-Edebiyat Fakültesi, Fizik Bölümü, 54187, Sakarya, Turkey*

[2] *Sakarya Üniversitesi, BIMAYAM Biyomedikal, Manyetik ve Yarıiletken Malzemeler Araştırma Merkezi, 54187, Sakarya, Turkey and*

[3] *School of Physics, University of Exeter, Stocker Road, Exeter EX4 4QL, UK*

(Dated: January 21, 2020)

Abstract

This study reports a theoretical examination of the structural, elastic, mechanical, electronic, phonon and electron-phonon interaction properties of the body-centered orthorhombic structure of NbPS by using the generalized gradient approximation of the density functional theory and the planewave *ab initio* pseudopotential method. An analysis of the elastic and mechanical properties reveals ductile nature of this compound. The electronic density of states at the Fermi energy is heavily contributed by d orbitals, revealing a more active role for transition metal Nb atoms in determining the lattice dynamical as well as the superconducting properties of NbPS. The phonon spectrum is characterized by anomalies in the lowest acoustic and lowest optical branches which are dominated by the vibrations of Nb atoms. The characteristic features in the electron and phonon spectra clearly suggest that the lowest branches of acoustic and optical nature are more involved in the process of scattering of electrons than the remaining ones due to their phonon anomalies and the significant existence of Nb d electrons at the Fermi level. From the integration of the Eliashberg spectral function, we obtain a value of average electron-phonon coupling constant $\lambda = 1.07$, confirming strong interaction between electrons and phonons. The computed value of superconducting critical temperature $T_c = 13.7$ K harmonizes very well with the experimentally reported value of 13.0 K.

PACS numbers: 63.20.kd, 71.15.Mb, 71.20.Lp, 74.25.Kc

I. INTRODUCTION

The ternary equiatomic transition metal compounds with the chemical formula TT$'$X (T: electron-poor transition metal, T$'$: electron-rich transition metal, X: P, As and Si) form a kind of metallic superconductors initially explored more than thirty years ago [1]. These metallic superconductors adopt two types of crystal structure: they usually occur either in the hexagonal ZrNiAl-type structure [2] or the orthorhombic TiNiSi-type structure [3]. Earlier experimental studies [1, 4–14] on reveal that hexagonal TT$'$X compounds usually possess considerably higher superconducting transition temperatures than their orthorhombic counterparts. On the other hand, in 2000, the orthorhombic MoRuP was reported to display a superconducting transition of 15.5 K [15], which is the highest among the ternary equiatomic transition metal superconductor family. Perhaps the most interesting member of intermetallic TT$'$X superconductors is ZrRuP since this exhibits polymorphism and can crystallize either in the hexagonal ZrNiAl-type structure (h-ZrRuP) or in the orthorhombic TiNiSi-type structure (o-ZrRuP). h-ZrRuP possesses a relatively high superconducting transition temperature (T_c) of around 13 K and a high upper critical field (Hc_2) of 17 T [1, 10, 14, 16, 17]. However, the superconducting transition of o-ZrRuP takes place at around 4 K [5, 10]. The large T_c difference between these two phases is not expected because h-ZrRuP and o-ZrRuP have almost equal density of states value at the Fermi level ($N(E_F)$), with former being slightly higher by 0.04 States/eV.atom [4, 8]. Therefore, according to the BCS mechanism of superconductivity [18, 19], the electron-phonon interaction must be essential in establishing higher T_c for h-ZrRuP than o-ZrRuP. Consequently, a fundamental theoretical study on the physical properties of these phases are required to explain their high T_c difference. Very recently, this genuinely prompted Bağcı and co-workers [20] to undertake *ab initio* pseudopotential calculations on the structural, electronic, elastic, mechanical, lattice dynamical and electron-phonon interaction properties of both phases in order to ascertain why h-ZrRuP is characterized by a higher T_c than o-ZrRuP. This theoretical work obviously reveals that the lattice of h-ZrRuP is softer than that of o-ZrRuP. This is responsible for the high T_c value of h-ZrRuP because soft phonon modes of h-ZrRuP make its electron-phonon coupling parameter (1.25) much larger than the corresponding value of 0.57 for o-ZrRuP and hence enhance its T_c value.

Another interesting ternary equiatomic compound is NbPS (niobium phosphorous sul-

phide) which crystalizes in body-centered orthorhombic structure [21, 22]. Different from TT′X-type compounds, this compound includes more non-metal atoms than transition metal atoms. Although NbPS is a non-metal rich compound, it is still metallic, transforming as a superconductor at around 12 K [21]. Shirotani and co-workers [23, 24] have investigated the electrical and magnetic properties of NbPS at low temperatures. They have reported that resistivity of this non-metal rich compound diminishes with decreasing temperature, and suddenly drops to zero at 13 K [23, 24]. The upper critical field value reported from these experiments [23, 24] is equal to 17 T. Although NbPS is a non-metal rich metallic superconductor, it is very challenging that these values almost equal to the corresponding values reported for the metal rich superconductor ZrRuP [1, 10, 14, 16, 17]. In spite of relatively high T_c value of 13 K, the $N(E_F)$ value of NbPS is derived to be 0.51 State/eV.atom from its specific heat measurement [23, 24]. This low value can not explain the relatively high T_c value of NbPS since its lower value may give rise to a lower value of electron-phonon coupling constant as well as a lower value of T_c according to the BCS mechanism of superconductivity [18, 19]. It is therefore reasonable to think that the relatively high T_c value of NbPS must arise from a strong electron-phonon interaction rather than its low $N(E_F)$ value. On the theoretical side, only tight-binding calculations [25] have been carried out on the electronic properties of NbPS. This theoretical work [25] has reported that the electronic state of this superconductor near the Fermi level is mostly d orbital in character. However, only electronic structure calculations are not enough to understand the formation of superconducting state for NbPS because of its low $N(E_F)$ value. Certainly, detailed phonon structure information is required to investigate the relatively high T_c of NbPS since several measurable physical properties of metallic systems originate from coupling between electrons and phonons. Specially, transport properties, like electrical or thermal resistivity, as well as the superconducting properties of metallic superconductors are governed by electron-phonon interaction.

The above reality prompts countenance for us to execute *ab initio* pseudopotential calculations on the structural, electronic, elastic, mechanical, lattice dynamical and electron-phonon interaction properties of the non-metal rich equiatomic superconductor NbPS. The calculation of structural and electronic properties for NbPS has been realized using the generalized gradient approximation of the density functional theory [26, 27]. In addition to structural and electronic calculations, elastic constant calculations have been carried out by

using the influential strain-stress method [28]. Based on the single crystal elastic constants, the elastic moduli such as bulk modulus, shear modulus, Young's modulus and Poisson's ratio have been worked out by using the Voigt-Reuss-Hill (VRH) notations [29–31]. Lattice dynamical calculations have been performed by utilizing a linear response approach, based on the *ab initio* pseudopotential method [26, 27]. Electron-phonon interaction calculations have been executed by combining the Migdal-Eliashberg theory and linear-response approach [26, 27, 32–35]. The rest of this theoretical work is organized in the following orders: the theoretical details are presented in Section 2, the results and related discussion are presented in Section 3 and finally, the summary of this work is made in Section 4.

II. METHOD

In this study, *ab initio* pseudopotential calculations have been carried out with use of the Quantum-Espresso simulation package [26, 27]. Ultrasoft pseudopotentials [36] are chosen to depict the electron-ion interaction. Exchange-correlation of the generalized gradient approximation of Perdew, Burke and Ernzerhof [37] is employed to calculate the interaction energy of electrons. The Brillouin zone integrations have been carried out with a $\boldsymbol{k}$ mesh of (6x6x6) for structural properties and (24x24x24) for electronic properties [38]. The cutoff energy for the plane-wave basis is 60 Ry, with an energy tolerance of 10^{-6} eV in the iterative solution of Kohn-Sham equations [39]. The crystal structure is totally relaxed until the force on each atom less than 0.01 eV/$\mathring{A}$. The lattice dynamical calculations have been executed by utilizing a linear response approach, based on the *ab initio* pseudopotential method [26, 27]. For the phonon calculations, we have conducted Brillouin zone integration by utilizing a set of 46 special $\boldsymbol{k}$ points. The calculation of dynamical matrices have been realized on a 3×3×3 $\boldsymbol{q}$-point mesh, and a Fourier interpolation is utilized to determine phonon frequencies for any taken $\boldsymbol{q}$ vector.

Electron-phonon interaction calculations have been executed by combining the Migdal-Eliashberg theory and a linear-response approach [26, 27, 32–35]. We have utilized a denser (24×24×24) $\boldsymbol{k}$ mesh for the electron-phonon interaction calculations, which need more careful treatment of the Fermi energy. According to the Migdal-Eliashberg theory, the phonon linewidth originates from the electron-phonon interaction by averaging over the Fermi sur-

face, which has the following form

$$\gamma_{\boldsymbol{q}j} = 2\pi\omega_{\boldsymbol{q}j} \sum_{\boldsymbol{k}nm} |\mathrm{g}^{\boldsymbol{q}j}_{(\boldsymbol{k}+\boldsymbol{q})m;\boldsymbol{k}n}|^2 \delta(\varepsilon_{\boldsymbol{k}n} - \varepsilon_F)\delta(\varepsilon_{(\boldsymbol{k}+\boldsymbol{q})m} - \varepsilon_F). \tag{1}$$

The Dirac delta functions represent energy conservation conditions. It is worth to mention that the calculation of electron-phonon matrix element ($\mathrm{g}^{\mathbf{q}j}_{(\mathbf{k}+\mathbf{q})m;\mathbf{k}n}$) has been performed self-consistently by using the linear response approach [26, 27]. The electron-phonon interaction spectral function (the Eliashberg spectral function ($\alpha^2F(\omega)$)) can be defined in terms of the phonon linewidth $\gamma_{\boldsymbol{q}j}$ of mode (qj) as

$$\alpha^2F(\omega) = \frac{1}{2\pi N(E_F)} \sum_{\mathbf{q}j} \frac{\gamma_{\mathbf{q}j}}{\hbar\omega_{\mathbf{q}j}} \delta\left(\omega - \omega_{\mathbf{q}j}\right). \tag{2}$$

The values of average electron-phonon coupling parameter and the logarithmically averaged phonon frequency $\omega_{\ln}$ can be derived from the integration of the Eliashberg spectral function by using following equations:

$$\lambda = 2\int \frac{\alpha^2F(\omega)}{\omega} d\omega, \tag{3}$$

$$\omega_{ln} = exp\left(2\lambda^{-1}\int_0^\infty \frac{d\omega}{\omega}\alpha^2F(\omega)ln\omega\right). \tag{4}$$

The superconducting critical temperature T_c is estimated from the Allen-Dynes modified McMillan equation [34, 35],

$$T_c = \frac{\omega_{\ln}}{1.2}\exp\left(-\frac{1.04(1+\lambda)}{\lambda - \mu^*(1+0.62\lambda)}\right), \tag{5}$$

where μ^* refers to a Coulomb pseudopotential which takes values between 0.10 and 0.16 [34, 35]. Following experimental studies on the NbPS superconductor [23, 24], its value is set to 0.10. Furthermore, the value of the average electron-phonon coupling parameter can be used to obtain the specific heat coefficient (γ) by the help of following equation:

$$\gamma = \frac{\pi^2}{3} n N_o k_B^2 N(E_F)(1+\lambda). \tag{6}$$

where n stands for the number of atoms per formula unit, N_o represents is Avogadro's number and k_B is the Boltzmann constant.

III. RESULTS

A. Structural and Electronic Properties

The studied compound NbPS exhibits a body-centered orthorhombic structure [21, 22] with space group Immm and point group D_{2h}(mmm) in which each primitive unit cell includes two formula units. The atoms occupy the following Wyckoff positions [21, 22]: two Nb atoms in the position 4(j) (1/2, 0, z_{Nb}), two P atoms in the position 4g (0, y_P, 0) and two S atoms in the position 4i (0, 0, z_S), where z_{Nb}, y_P, and z_S refer to inner coordinates. Consequently, the crystal structure of NbPS is characterized by three lattice parameters (a, b, c) and three inner coordinates (z_{Nb}, y_P, z_S). As the first step of our *ab initio* calculations, we have achieved the structural optimization under the condition of minimum total energy and vanishing forces on atoms in order to specify its lattice parameters (a, b, c) and inner coordinates (z_{Nb}, y_P, z_S). Then, the bulk modulus (B) and its pressure derivative ($B^{'}$) have been estimated by minimizing the crystal total energy for different values of crystal volume by means of Murnaghan equation of state. Tab. I presents the calculated values of lattice parameters, inner coordinates, bulk modulus and its pressure derivative along with existing experimental data [21, 22, 24] for lattice parameters and inner coordinates. Generally speaking, the calculated values of lattice parameters and inner coordinates significantly harmonize with their corresponding experimental values [21, 22, 24]. In particular, the relative errors between the calculated lattice parameters and their experimental values [21, 22, 24] are less than 1% while the calculated values of inner coordinates are almost equal to their corresponding experimental values [21, 22]. There are no experimental results available for us to compare our results for bulk modulus and its pressure derivative. The crystal structure of NbPS is plotted in Fig. 1 by using the calculated lattice parameters and the calculated inner coordinates. This crystal structure exhibits several interesting features. Each niobium atom is in eight-fold coordination formed by four sulfur and four phosphorus atoms. The average bond-length value of Nb-S bonds is 2.598 $\mathring{A}$, comparing very well with its experimental value [21, 22] of 2.596 $\mathring{A}$. The interatomic distance Nb-P amounts to 2.598 $\mathring{A}$ which harmonizes with its experimental value [21, 22] of 2.582 $\mathring{A}$. As can be seen from Fig. 1, the P atoms form perpetual strings in the **y**-axis with successive short (2.256 $\mathring{A}$) and long (2.479 $\mathring{A}$) distances. These values are also comparable with their experimental values [21, 22]

of 2.221 and 2.504 $\mathring{A}$. Finally, the Nb atoms form a dimer in the **z**-axis with the bond-length value of 2.991 $\mathring{A}$. This value is almost equal to the sum of the corresponding atomic radii value of 2.90 $\mathring{A}$, signaling a strong Nb-Nb dimer in NbPS.

The calculated electronic band structure of NbPS is displayed in Fig. 2 (a) along several symmetry lines within the Brillouin zone of the body-centered orthorhombic lattice (see Ref. [41] for the Brillouin zone). The energy scale is defined by setting the Fermi level at $E_F = 0$. The overall band structure looks similar to the tight-binding results presented by Keszler and Hoffmann [25]. According to Fig. 2 (a), this compound is a three-dimensional metal; at least one band with significant dispersion crosses the Fermi level. In order to explain the orbital character of electronic bands, the total and partial density of states (DOS and PDOS) are presented together in Fig. 2 (b). The DOS can be divided into two regions separated by a very small gap of 0.16 eV: one block at lower energies extending from -16.0 to -7.91 eV and other one from -7.75 eV up to energies above the Fermi level. The peak at -13.2 eV in the first region is mainly formed by S 3s orbitals with lesser but remarkable additives from P 3s, Nb 5p and Nb 4d orbitals. The valence band located between -12.0 and -7.91 eV originates from mixed P 3s, P 3p and Nb 4d states with the maximum contribution coming from the first one. In the second region, we have observed that Nb 4d states are significantly hybridized with S 3p and P 3p states in the energy window from -7.75 to -1.25 eV, confirming the presence of Nb-S and Nb-P strong bondings. The dominance of Nb 4d states is found in the energy range from -1.25 eV to 4 eV. Therefore, the electronic bands of NbPS near the Fermi level are of mostly d orbital character with a slight degree of hybridization with the p states of non-metal atoms. The density of states at the Fermi level is $N(E_F) = 0.502 \frac{States}{eV.atom}$ which almost equals to its experimental value of $0.51 \frac{States}{eV.atom}$ [23, 24]. The low $N(E_F)$ value of NbPS is the first sign of strong electron-phonon interaction due its relatively high T_c value. The contributions of Nb, P, and S atoms to the value of $N(E_F)$ are roughly 77%, 11%, and 12%, respectively. It is worth to mention that the most dominant contribution to $N(E_F)$ comes from Nb 4d states within roughly 74%. On the other hand, the p states of non-metal atoms contribute almost equally to the value of $N(E_F)$ within approximately 9%. In the light of above discussion, we can conclude that d states of transition metal atoms play a dominant role in the metallic nature of the investigated compound.

For a better understanding of the electronic structure, the Brillouin zone (Fig. 3 (a)) and Fermi surfaces (Fig. 3 (b),(c) and (d)) of body-centered orthorhombic NbPS are illustrated.

Even though it seems that there are three electronic bands crossing the Fermi energy level, the third band is barely touching this level between Y-Γ direction. First Fermi-crossing band has mainly hole-pocket like characteristics (see Fig. 2 (a) and Fig. 3 (b)) while the other two Fermi-crossing bands are dominated by electron-pocket like characteristics (see Fig. 2 (a) and Fig. 3 (c),(d)). The first Fermi-crossing electronic band produces two hole-like pockets around the zone boundary Y point that can be seen from Fig. 3 (b). Second Fermi-crossing band constructs a closed Fermi surface sheet around the Z high-symetry point that shows some nesting. All the Fermi surface pockets around the symmetry points except the Γ high-symmetry point show hole-like behaviour. Although multiple electronic bands cross the Fermi level and construct Fermi surface sheets, none of them shows a large nesting property which suggests the picture of conventional superconductivity.

B. Elastic and Mechanical Properties

The elastic properties of superconducting compounds must be investigated since the long-wavelength phonon spectra is closely associated with the elastic properties of material and the source of BCS type superconductivity is the electron-phonon interaction. In this study, elastic constant calculations have been determined by using the strain-stress method as exercised in the thermo$_{pw}$ code [28]: a set of small strains is applied on the crystal lattice and then the lattice containing the atoms are totally relaxed to obtain the corresponding stress. Single crystal elastic constants are derived from the determined strain-stress relations. For the orthorhombic lattice, there are nine independent single crystal elastic constants; namely, C_{11}, C_{22}, C_{33}, C_{44} C_{55}, C_{66}, C_{12}, C_{13} and C_{23}. The calculated values of these elastic constants are presented in Tab. II. The value of C_{22} is much larger than the corresponding values of remaining elastic constants which means that the studied superconductor is very incompressible along the **y** axis. It is well known that C_{11}, C_{22} and C_{33} represent the linear compression along crystal axis while C_{44}, C_{55} and C_{66} are connected to shear deformation. Since the values of C_{11}, C_{22} and C_{33} are significantly larger than the corresponding values of C_{44}, C_{55} and C_{66}, the superconductor NbPS offers stronger resistance to the unidirectional compression than the shear deformation. For a mechanically stable orthorhombic system, elastic constants need to meet the following stability conditions [40]:

$$C_{ii} > 0 \quad (i = 1, 6), \qquad C_{11} + C_{22} - 2C_{12} > 0,$$

$$C_{22}+C_{33}-2C_{23}>0, \qquad C_{11}+C_{33}-2C_{13}>0,$$

$$C_{11}+C_{22}+C_{33}+2C_{12}+2C_{13}+2C_{23}>0.$$

Elastic constants presented in Tab. II totally satisfy the above stability conditions which means that the superconductor NbPS is mechanically stable in its orthorhombic crystal structure.

The polycrystalline moduli are more remarkable than the second order single crystal elastic constants and can represent mechanical properties. The bulk modulus reflects the resistance to the alteration of volume by external pressure while shear modulus stands for the resistance to convertible deformation under shear stress. Young's modulus represents the resistance to uniaxial tensions. Based on the single crystal elastic constants, the elastic moduli such as bulk modulus (B), shear modulus (G), Young's modulus (E) and Poisson's ratio (σ) can be determined by using the Voigt-Reuss-Hill (VRH) notations [29–31]. The Voigt notation [29] represents the upper bound of mechanical modulus in terms of the uniform strain, and the Reuss notation [30] refers to the lower bound in terms of the uniform stress. The Hill notation [31] is the arithmetic average of Voigt and Reuss notations. Using the VRH notations, the value of B, G, E and σ can be obtained from the following formulas:

$$B_H = \frac{B_V+B_R}{2}, \quad G_H=\frac{G_V+G_R}{2}, \quad E=\frac{9B_HG_H}{3B_H+G_H}, \quad \sigma=\frac{(3B_H-2G_H)}{(6B_H+2G_H)}, \tag{7}$$

$$B_V = \frac{1}{9}(C_{11}+C_{22}+C_{33}+2C_{12}+2C_{13}+2C_{23}), \tag{8}$$

$$G_V = \frac{1}{15}(C_{11}+C_{22}+C_{33}+3C_{44}+3C_{55}+3C_{66}-C_{12}-C_{13}-C_{23}, \tag{9}$$

$$B_R = \frac{1}{(S_{11}+S_{22}+S_{33})+2(S_{12}+S_{13}+S_{23})}, \tag{10}$$

$$G_R = \frac{15}{4(S_{11}+S_{22}+S_{33})-4(S_{12}+S_{13}+S_{23})+3(S_{44}+S_{55}+S_{66})}, \tag{11}$$

where S_{ij} ($=C_{ij}^{-1}$) are the elastic compliance constants. The calculated values of B_{VRH}, G_{VRH}, B_H/G_H and σ are listed in Tab. III. Although no experimental data are available for the elastic moduli of NbPS, the calculated value of B_H is almost equal to the corresponding one obtained by fitting to the Murnaghan equation of states (see Tab. I), validating the trustworthiness of our calculations. As can be sen from Tab. III, the shear modulus of NbPS is much smaller than its bulk modulus, which implies that shape deformation is easier to emerge than volume change for this superconductor. Pugh [42] suggests that the ratio of bulk to shear modulus (B_H/G_H) can be used to define ductility or brittleness of materials. If

this ratio is greater than its critical value of 1.75, materials exhibit ductile nature, otherwise they exhibit brittle nature. The value of this ratio for NbPS is 1.93, which means that this superconductor has ductile nature. In addition to the B_H/G_H ratio, the Poisson's ratio (σ) [43] can be used to define the brittleness and ductility of materials. If this ratio greater than its critical value of 0.26, materials are ductile, or else they are brittle. This ratio is greater than 0.26 for NbPS which also confirms that the studied compound is ductile.

C. Phonons and Electron-Phonon interaction

First, we will focus on the zone-center phonon modes of the NbPS superconductor since they play an appreciable role in Raman scattering and infrared absorption. According to the group theoretical analysis, the zone-center optical phonon modes of NbPS can be expressed as

$$\Gamma(D_{2h}) = A_g + B_{1g} + 2B_{2g} + 3B_{3g} + 2B_{1u} + 2B_{2u} + B_{3u},$$

where all the phonon modes are non-degenerate with u and g corresponding to infrared active and Raman active modes, respectively. The egienvector representations of zone-center vibrations are illustrated in Fig. 4, together with their frequencies and electron-phonon coupling constants. The largest electron-phonon coupling constant is observed for the lowest optical phonon mode with a value of 0.448. This result is not surprising for us due to two reasons. First, this phonon mode involves opposing vibrations of Nb atoms which dominate the electronic bands with their d states in the vicinity of the Fermi level. Secondly, its low frequency gives rise to a larger electron-phonon interaction according to the factor $\frac{1}{\omega}$ in the integral formula of Eq. 3. The total electron-phonon coupling parameter for the zone-center phonon modes is larger than 0.9 which is the second sign of strong coupling between electrons and phonons in NbPS.

Up to now, only zone-center phonon modes are presented and discussed but the knowledge of full phonon spectrum and phonon density of states plays a vital role in understanding the electron-phonon coupling mechanism. Therefore, the calculated phonon spectrum of NbPS is presented in Fig. 5 (a) along the high-symmetry lines within the Brillouin zone of the body-centered orthorhombic lattice. Interesting features can be deduced from a simple assessment of this phonon spectrum. First, the appearance of only real positive frequencies in this spectrum suggests the dynamical stability of NbPS in the body-centered orthorhombic

structure. Secondly, the low-frequency region contains a set of six phonon bands extending up to around 6.15 THz, separated by a narrow gap of 0.05 THz from the high frequency region that includes twelve optical phonon bands, lying between 6.20 and 13.20 THz. This narrow gap is probably a consequence of small mass difference between S and P atoms. Thirdly, three optical and three acoustic branches in the low frequency region are completely dispersive which leads to a strong overlap between them. In order to specify the role of all phonon branches, the total and partial density of states for NbPS are presented in Fig. 5 (b). Analyzing the partial DOS one can find that, as anticipated, Nb as the heaviest atom in this superconductor dominates the three acoustic and three optical bands in the low frequency region. However, much smaller S and P contributions are present in this frequency region. Therefore, it will be expected that Nb-related vibrations play a highly significant role in the formation of superconducting state for NbPS. In other words, they may couple strongly with the electrons at the Fermi energy. We will further discuss this when presenting the calculated Eliashberg spectral function. The DOS features between 6.20 and 11.10 THz are mainly characterized by the hybridized vibrations of S and P atoms which is probably due to their similar atomic masses. Although P-related vibrations occur over the whole range of phonon frequencies, Nb-related and S-related vibrations almost disappear above 11.10 THz. Therefore, the partial DOS exhibits a dominance of P atoms above this frequency.

The most significant feature in the phonon spectrum of NbPS is the softening of the lowest optical phonon branch (B_{3g}) along the Γ-X, Γ-R, and Γ-X_1 symmetry directions. Along these symmetry directions, the frequency of this phonon band considerably decreases with increasing wave vector. Therefore, this optical band crosses three acoustic branches along these symmetry directions and has a lower frequency than them. This behavior of the lowest B_{3g} mode is known as a phonon anomaly in the literature. This significant phonon anomaly of the lowest B_{3g} mode appears to be very substantial in the formation of superconducting state for NbPS since previous theoretical studies on LNi_2B_2C (L = Lu, Sc) and YPd_2B_2C superconductors [44, 45] have shown that a significant phonon anomaly causes large electron-phonon interaction. In order to reveal a positive relationship between the anomalous dispersion of the lowest B_{3g} mode and its electron-phonon coupling constant, we show together its electron-phonon coupling constant and frequency in Fig. 6 (a) along the R-Γ-X_1 direction. The most salient characteristic of this phonon band is that its electron-phonon coupling parameter approaches the largest value of 3.05 at the R point, where its

frequency equals to 1.426 THz. This large value is the third sign of strong electron-phonon interaction in NbPS. The eigenvector representation of the lowest B_{3g} mode at the R point is displayed in Fig. 6 (b). This phonon mode has a dimer rocking character due to the opposing motion of Nb dimer atoms along the [010] direction. This character is not surprising since Nb d electrons dominate the electronic states close to the Fermi level. The eigenvector representation of this phonon mode leads to considerable changes in the overlap of electronic orbitals of neighboring atoms, giving rise to a large electron-phonon coupling parameter. It is worth to mention that the lowest optical phonon branch also exhibits a phonon anomaly along the Y-X, S-R and Z-W symmetry directions. The anomalous dispersion of this phonon branch along these symmetry directions makes its electron-phonon coupling parameter quite large. Especially near the Z-W direction (at $\boldsymbol{q} \simeq 0.20\ \overline{ZW}$), a particular phonon softening can be observed. This phonon softening happens along the Fermi surface electron nesting which can be seen in Fig. 3 (c) which was mentioned before. The Fermi surface nesting and the phonon softening around this $\boldsymbol{q}$ supports superconductivity. Once again, Nb-related vibrations dominate the eigenvector representation of this phonon branch.

To elaborate the strengths with which different phonon modes couple to electrons and hence are capable of affecting the electron-phonon interaction properties most, the Eliashberg spectral function ($\alpha^2F(\omega)$) of NbPS is illustrated in Fig. 7 along with the frequency accumulated value of the electron-phonon coupling constant λ. A critical comparison of this spectral function and phonon DOS reveals that the former one is enhanced relative to latter one in the frequency range from 1.69 to 3.51 THz. It is worth to mention that phonon modes below 3.51 THz contribute almost 57% of the average electron-phonon coupling constant. This large contribution confirms that the softening of lowest optical and acoustic branches plays an essential role in the transition from the normal state to the superconducting state since they have a dimer rocking character due to the opposing motion of Nb dimer atoms, dominating the electronic states near the Fermi level with their d orbitals. In addition to the contribution of low frequency phonon modes, phonon modes between 3.51 and 6.15 THz contribute to λ in the order of 17%, while the remaining 26% of λ arises from phonon modes above the narrow gap region.

In the light of above discussion, we can emphasize that the lowest optical and acoustic phonon branches are more involved in the process of scattering of electrons than the remaining phonon branches because of their phonon anomalies. The calculated values of density of

states at the Fermi level ($N(E_F)$), logarithmically averaged frequency (ω_{ln}), average electron-phonon coupling constant (λ), superconducting critical temperature (T_c), and specific heat coefficient (γ) are listed in Tab. IV, together with the experimental values of $N(E_F)$, λ, T_c and γ. Generally speaking, the calculated values of $N(E_F)$, λ, T_c and γ are comparable with the experimental values. In particular, the calculated λ from the integration of $\alpha^2F(\omega)$ is 1.07, being the final sign of strong coupling between electrons and phonons for NbPS. It is worth to mention that the λ value of NbPS is smaller than the corresponding value of 1.25 for h-ZrRuP [20]. This result is expected because the $N(E_F)$ value of 0.61 States/eV.atom for h-ZrRuP [20] is higher than that of NbPS and a higher value of $N(E_F)$ can account for a higher λ according to the BCS mechanism of superconductivity [18, 19].

IV. SUMMARY

To summarize, we have reported a theoretical examination of the structural, electronic, elastic, mechanical, phonon and electron-phonon interaction properties of the body-centered orthorhombic structure of NbPS by using the generalized gradient approximation of the density functional theory and the planewave *ab initio* pseudopotential method. The calculated values of lattice parameters and inner coordinates considerably harmonize with their experimentally reported ones. The electronic bands near the Fermi level are of mostly d orbital character with much smaller contributions from the p orbitals of non-metal atoms. This result reveals that Nb 4d states play dominant roles in the conduction properties of the studied superconductor. An analysis of elastic constants and elastic moduli ascertains the ductile nature of NbPS.

In addition to electronic and elastic properties, lattice dynamical properties of NbPS are presented and discussed in detail. The most interesting feature in the phonon dispersion curves of NbPS is the softening of (i.e. shows anomaly in) the lowest acoustic and lowest optical phonon branches. We have shown that this phonon anomaly leads to strong electron-phonon interaction in the studied superconductor. Analyzing the partial phonon DOS, we find that the most of the lattice vibrations below 6.02 THz mainly originate from the heavier Nb atoms while most of lattice vibrations between 6.20 and 11.10 THz come from the coupled motion of lighter S and P atoms. Nb and S atoms remain almost silent above 11.10 THz which is dominated by the vibrations of lightest P atoms. This picture reveals that Nb-

related low-frequency vibrations have the potential to be more involved in the process of scattering of electrons than the remaining vibrations.

The calculation of the Eliashberg spectral function for NbPS has been made by combining the Migdal-Eliashberg theory and a linear-response approach. A critical comparison of the Eliashberg spectral function and phonon DOS indicates that the former one is enhanced relative to latter one in the frequency range from 1.69 to 3.51 THz. Phonon modes lying in this frequency region contribute almost 57% of the average electron-phonon coupling constant. This large contribution confirms that the lowest acoustic and optical phonon modes dominated by the vibrations of Nb atoms contribute strongly in thr coupling mechanism due to their phonon anomalies. From integration of the Eliashberg spectral function, we obtain the value of average electron-phonon coupling constant $\lambda = 1.07$ which suggests that NbPS is a conventional phonon-mediated superconductor with strong electron-phonon coupling. Finally, the calculated value of the superconducting critical temperature is $T_c = 13.7$ K, which compares very well with its experimental value of 13.0 K. We, therefore, conclude that the conventional electron-phonon coupling theory is sufficient to explain the formation of superconducting state for the equiatomic NbPS compound.

Acknowledgement

Numerical calculations were performed using the Intel Nehalem (i7) cluster (ceres) at the University of Exeter.

[1] H. Barz, H. C. Ku, G. P. Meisner, Z. Fisk, and B. T. Matthias, Ternary transition metal phosphides: High-temperature superconductors, Proc. Natl. Acad. Sci. USA **77**, 3132 (1980).

[2] A. E. Dwight, M. H. Mueller, R. A. Conner, Jr., J. W. Downey, H. Knott, Ternary Compounds with the Fe_2P-Type Structure, Trans. Met. Soc. AIME **242**, 2075 (1968).

[3] C. B. Shoemaker, D. P. Shoemaker, A ternary alloy with $PbCl_2$-type structure: TiNiSi(E), Acta Crystallogr. **18**, 900 (1965).

[4] G. R. Stewart, G. P. Meisner and H. C. Ku, Superconductivity in d- and f-Band Metals edited by W. Buckel and W. Weber (Karlsruhe: Kernforschungszentrum) p. 331 1982.

[5] R. Muller, R. N. Shelton, J. W. Richardson, Jr. and R. A. Jacobson, Superconductivity and crystal structure of a new class of ternary transition metal phosphides TT/t$'$P (T: Zr, Nb, Ta and T/t$'$: Ru, Rh), J. Less-Common Met. **92**, 177 (1983).

[6] G. P. Meisner and H. C. Ku, The superconductivity and structure of equiatomic ternary transition metal pnictides, Appl. Phys. A **31**, 201 (1983).

[7] G. P. Meisner, H. C. Ku and H. Barz, Mater. Res. Bull. **18**, 983 (1983).

[8] H. Keiber, H. Wuhl, G. P. Meisner and G. R. Stewart, Phonon anomalies in ZrRuP, J. of Low. Temp. Phys. **55**, 11 (1984).

[9] W. Xian-Zhong, B Chevalier, J Etourneau, P Hagenmuller, New superconducting equiatomic ternary silicides MIrSi (M = Y, Zr, Hf) with TiNiSi-type structure (anti-$PbCl_2$) Mat. Res. Bull., **20**, 517 (1985).

[10] I. Shirotani, N. Ichihashi, K. Nozawa, M. Kinoshita, T. Yagi, K. Suzuki, T. Enoki, Superconductivity of ZrRuP, Japan. J. Appl. Phys. **32**, 695 (1993).

[11] I. Shirotani, K. Tachi, N. Ichihashi, T. Adachi, T. Kikegawa and O. Shimomura, Phase-transition of ZrRuP at high-temperatures and high-pressures, Physics Letters A **205**, 77 (1995).

[12] I. Shirotani, K. Tachi, K. Takeda, S. Todo, T. Yagi, and K. Kanoda, Superconductivity of ZrRuSi prepared at high-pressure, Phys. Rev. B **52**, 6197 (1995).

[13] H. Salamati, F. S. Razavi and G. Quirion, Effect of pressure on the superconductivity of ZrRuP, Physica C **292**, 79 (1997).

[14] I. Shirotani, K. Tachi, Y. Konno, S. Todo and T. Yagi, Superconductivity of the ternary

ruthenium compounds HfRuP and ZrRuX (X = P, As, Si or Ge) prepared at a high pressure, Phil. Mag. B **79**, 767 (1999).

[15] I. Shirotani, M. Takeya, I. Kaneko, C. Sekine, and T. Yagi, Superconductivity of MRuP and MNiP (M= Mo or W) prepared at high pressure, Solid State Commun. **116**, 683 (2000).

[16] I. Shirotani, Y. Konno, D. Kato, C. Sekine, S. Todo and T. Yagi, Superconductivity of ternary equiatomic compounds with T_c of above 10 K, Jpn. J. Appl. Phys. **39**, 525 (2000).

[17] I. Shirotani, D. Kato, A. Nishimoto and T. Yagi, Superconductivity and crystal structure of $ZrRu_{1-x}Rh_xP$ alloys prepared at high pressure, J. Phys.-Condens. Matter **13**, 9393 (2001).

[18] J. Bardeen, L. N. Cooper, J. R. Schrieffer, Theory of Superconductivity, Phys. ReV. **108**, 1175 (19657).

[19] W. L. McMillan, Transition temperature of strong-coupled superconductors, Phys. Rev. **167**, 331 (1968).

[20] S. Bağcı, M. Cin, H. Y. Uzunok, Ertuğrul Karaca, H. M. Tütüncü, and G. P. Srivastava, Investigating the normal state and superconducting state properties of orthorhombic and hexagonal ZrRuP: A first-principles study, Phys. Rev. B **100**, 184507 (2019).

[21] P. C. Donohue and P. E. Bierstedt, Synthesis, crystal structure, and superconducting properties of niobium phosphorus sulfide, niobium phosphorus selenide and tantalum phosphorus sulfide, Inorg. Chem. **8**, 2690 (1969).

[22] C. P. Poole Jr., Handbook of superconductivity, first ed.,Academic Press, San diego, 2000, Chap. 6, p. 209.

[23] I. Shirotani, H. Kadoya, C. Sekine, S. Todo, T. Yagi, Y. Nakazawa and K. Kanoda, Superconductivity of niobium phosphorous sulphide, NbPS, prepared at high pressure, J. Phys.: Condens. Matter **11**, 6231 (1999).

[24] I. Shirotani, Superconductivity of Ternary Metal Compounds Prepared at High Pressures, Bull. Chem. Soc. Jpn. **76**, 1291 (2003).

[25] D. A. Keszlert and R. Hoffmann, Bonding and Electronic Structure of Superconducting NbPS, J. Am. Chem. Soc. **109**, 118 (1987).

[26] P. Giannozzi, S. Baroni, N. Bonini, M. Calandra, R. Car, C. Cavazzoni, D. Ceresoli, G. L. Chiarotti, M. Cococcioni, I. Dabo, A. Dal Corso, S. de Gironcoli, S. Fabris, G. Fratesi, R. Gebauer, U. Gerstmann, C. Gougoussis, A. Kokalj, M. Lazzeri, L. Martin-Samos, N. Marzari, F. Mauri, R. Mazzarello, S. Paolini, A. Pasquarello, L. Paulatto, C. Sbraccia, S. Scandolo,

G. Sclauzero, A. P. Seitsonen, A. Smogunov, P. Umari, R. M. Wentzcovitch, QUANTUM ESPRESSO: a modular and open-source software project for quantum simulations of materials, J. Phys.: Condens. Matter **21**, 395502 (2009).

[27] P. Giannozzi, O. Andreussi, T. Brumme, O. Bunau, M. Buongiorno Nardelli, M. Calandra, R. Car, C. Cavazzoni, D. Ceresoli, M. Cococcioni, N. Colonna, I. Carnimeo, A. Dal Corso, S. de Gironcoli, P. Delugas, R. A. DiStasio Jr., A. Ferretti, A. Floris, G. Fratesi, G. Fugallo, R. Gebauer, U. Gerstmann, F. Giustino, T. Gorni, J. Jia, M. Kawamura, H.-Y. Ko, A. Kokalj, E. Kkbenli, M. Lazzeri, M. Marsili, N. Marzari, F. Mauri, N. L. Nguyen, H.-V. Nguyen, A. Otero-de-la-Roza, L. Paulatto, S. Ponc, D. Rocca, R. Sabatini, B. Santra, M. Schlipf, A. P. Seitsonen, A. Smogunov, I. Timrov, T. Thonhauser, P. Umari, N. Vast, X. Wu, and S. Baroni, Advanced capabilities for materials modelling with Quantum ESPRESSO, J. Phy.: Condensed Matter **29**, 465901 (2017).

[28] A. Dal Corso, Elastic constants of beryllium: a first-principles investigation, J. Phys.: Condens. Matter **28**, 075401 (2016).

[29] W. Voigt, Lehrbuch der Kristallphysik, Leipzig, Taubner, (1928).

[30] A. Reuss, Berechnung der Fließgrenze von Mischkristallen auf Grund der Plastizitätsbedingung für Einkristalle, Z. Angew. Math. Mech. **9**, 49 (1929).

[31] R. Hill, The elastic behaviour of a crystalline aggregate, Proceedings of the Physical Society Section A **65**, 349 (1952).

[32] A. B. Migdal, Interaction between electrons and lattice vibrations in a normal metal, Zh. Eksp. Teor. Fiz. **34**, 996 (1958).

[33] G. M. Eliashberg, Interaction between electrons and lattice vibrations in a superconductor, Sov. Phys. JETP. **11**, 696 (1960).

[34] P. B. Allen and R. C. Dynes, Transition temperature of strong-coupled superconductors reanalyzed, Phys. Rev. B **12**, 905 (1975).

[35] P. B. Allen and R. C. Dynes, Superconductivity at very strong coupling, J. Phys. C: Solid State Physics **8**, L158 (1975).

[36] D. Vanderbilt, Soft self-consistent pseudopotentials in a generalized eigenvalue formalism, Phys. Rev. B **41** 7892 (R) (1990).

[37] J. P. Perdew, K. Burke, and M. Ernzerhof, Generalized Gradient Approximation Made Simple, Phys. Rev. Lett. **77**, 3865 (1996).

[38] H. J. Monkhorst and J. D. Pack, Special points for Brillouin-zone integrations, Phys. Rev. B **13**, 5188 (1976).

[39] W. Kohn and L. J. Sham, Self-Consistent Equations Including Exchange and Correlation Effects, Phys. Rev. **140**, A1133 (1965).

[40] Z.-j. Wu, E.-j. Zhao, H.-p. Xiang, X.-f. Hao, X.-j. Liu, J. Meng, Crystal structures and elastic properties of superhard IrN_2 and IrN_3 from first principles, Phys. Rev. B **76**, 054115 (2007).

[41] W. Setyawan and S. Curtarolo, High-throughput electronic band structure calculations: Challenges and tools, Computational Materials Science **49**, 299 (2010).

[42] S. Pugh, XCII. Relations between the elastic moduli and the plastic properties of polycrystalline pure metals, Phil. Mag. **45**, 823 (1954).

[43] J. Haines, J. Leger, G. Bocquillon, Synthesis and design of superhard materials, Annu. Rev. Mater. Res. **31**, 1 (2001).

[44] H. M. Tütüncü, H. Y. Uzunok, Ertuğrul Karaca, G. P. Srivastava, S. Özer, and Ş. Uğur, Ab-initio investigation of BCS-type superconductivity in $LuNi_2B_2C$-type superconductors, Phys. Rev. B **92**, 054510 (2015).

[45] H. M. Tütüncü, Ertuğrul and G. P. Srivastava, Electron-phonon interaction and superconductivity in the borocarbide superconductor $ScNi_2B_2C$, Phil. Mag. **97** 2669 (2017).

TABLE I: The calculated values of lattice constants (a, b and c), bulk modulus (B), the pressure derivative of bulk modulus ($B^{'}$) and inner parameters (z_{Nb}, y_P and z_S) for NbPS. Available experimental values are also listed. [Need to mention units]

Source	$a(\AA)$	$b(\AA)$	$c(\AA)$	B (GPa)	$B^{'}$	z_{Nb}	y_P	z_S
NbPS	3.451	4.736	11.996	139.10	4.74	0.125	0.262	0.287
Experimental [21, 22]	3.438	4.725	11.880			0.123	0.265	0.288
Experimental [24]	3.443	4.733	11.919					

TABLE II: Theoretical values of the nine independent single crystal elastic constants (C_{ij} in GPa) for NbPS. [Need to mention units]

Source	C_{11}	C_{12}	C_{13}	C_{22}	C_{23}	C_{33}	C_{44}	C_{55}	C_{66}
This work	195.16	74.05	105.22	299.39	86.12	256.88	46.41	99.38	74.18

TABLE III: Theoretical values of isotropic bulk modulus B_{VRH}, shear modulus G_{VRH}, Young's modulus E (all in GPa), B_H/G_H ratio and Poisson's ratio (σ) for NbPS, derived from the nine independent single crystal elastic constants.[Need to mention units]

Source	B_V	B_R	B_H	G_V	G_R	G_H	E	B_H/G_H	σ
This work	142.05	138.90	140.13	76.20	69.44	72.93	186.53	1.93	0.278

TABLE IV: The calculated values of density of states at the Fermi level ($N(E_F)$), logarithmically averaged frequency ($\omega_{\ln}$), average electron-phonon coupling constant (λ), superconducting critical temperature (T_c), and electronic specific heat coefficient (γ). For comparison, the experimental values of $N(E_F)$, λ, T_c and γ are also included.

Source	$N(E_F)$ (States/eV.atom)	ω_{ln} (K)	λ	T_c (K)	$\gamma(\frac{mJ}{molK^2})$
This work	0.502	179.13	1.07	13.7	7.3
Experimental [23, 24]	0.51		0.81	13.0	6.5

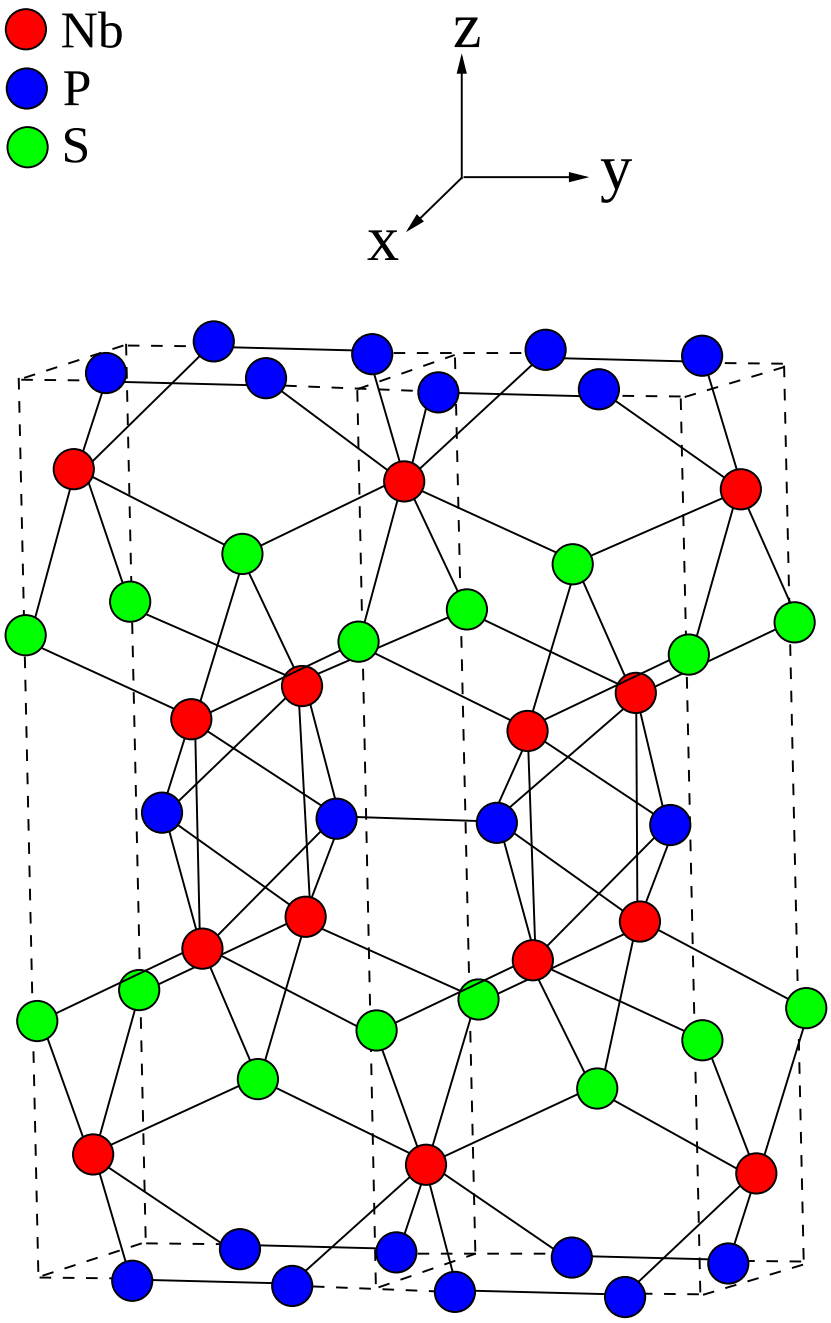

FIG. 1: The body-centered orthorhombic crystal structure of NbPS. Each Nb atom coordinates with four S atoms and four P atoms while each S atom coordinates with four Nb atoms. Each P atom coordinates with four Nb atoms and one P atom.

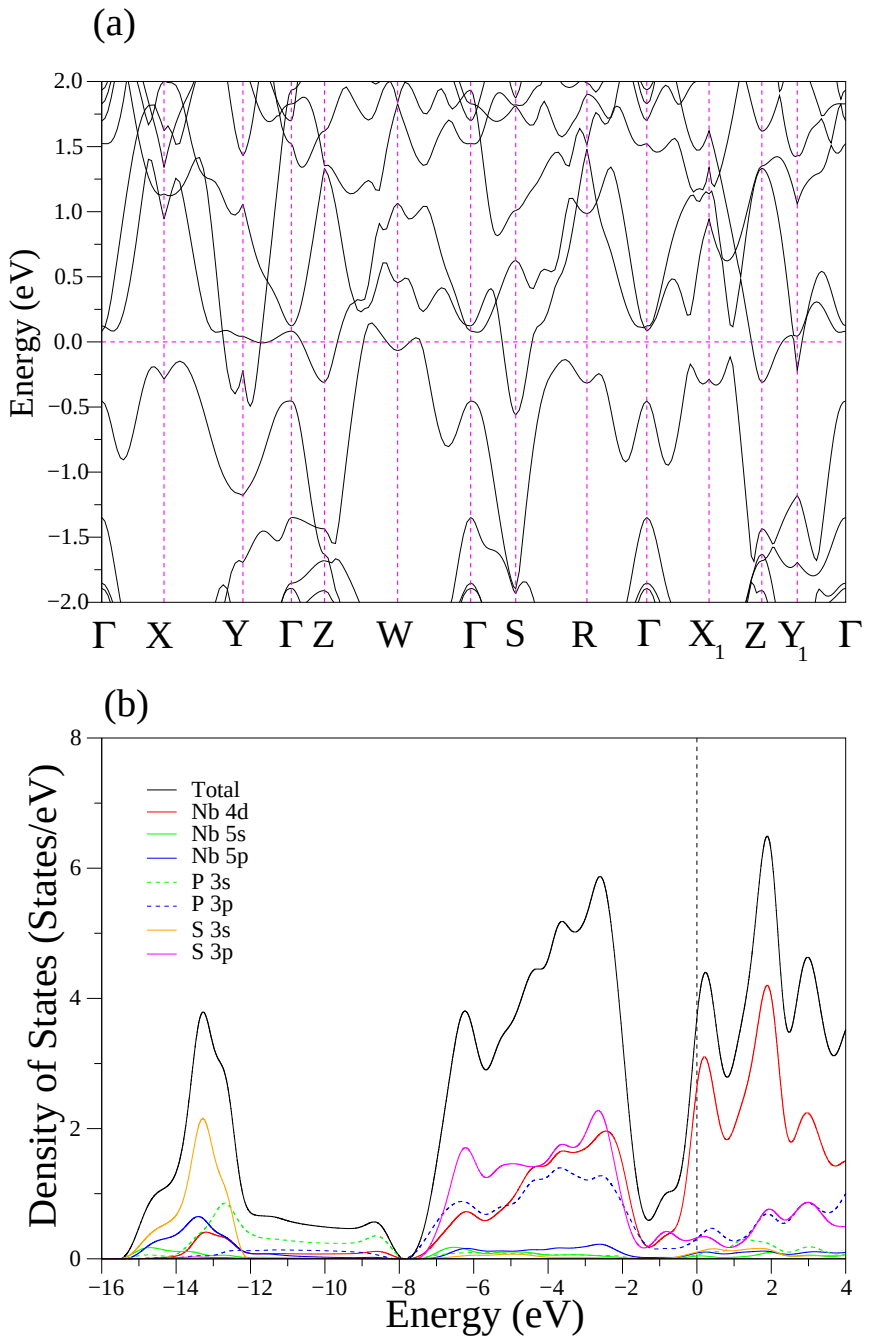

FIG. 2: (a) The calculated electronic band structure for NbPS plotted along the high symmetry directions of the body-centered orthorhombic Brillouin zone. The Fermi level is fixed at 0 eV. The high–symmetry points in the Brillouin zone in Cartesian coordinates are: X = $\frac{2\pi}{a}$((0.50+0.50$\frac{a^2}{c^2}$), 0.00, 0.00), Y = $\frac{2\pi}{a}$(0.00, $\frac{a}{b}$(0.50+0.50$\frac{b^2}{c^2}$), 0.00), Z = $\frac{2\pi}{a}$(0.00, 0.00, $\frac{a}{c}$), W = $\frac{2\pi}{a}$(0.50, 0.50$\frac{a}{b}$, 0.50$\frac{a}{c}$), S = $\frac{2\pi}{a}$(0.00, 0.50$\frac{a}{b}$, 0.50$\frac{a}{c}$), R =$\frac{2\pi}{a}$(0.50, 0.00, 0.50$\frac{a}{c}$), X_1 =$\frac{2\pi}{a}$((0.50-0.50$\frac{a^2}{c^2}$), 0.00, $\frac{a}{c}$) and Y_1 =$\frac{2\pi}{a}$(0.00, $\frac{a}{b}$(0.50-0.50$\frac{b^2}{c^2}$), $\frac{a}{c}$) (b) Total and partial electronic density of states for NbPS.

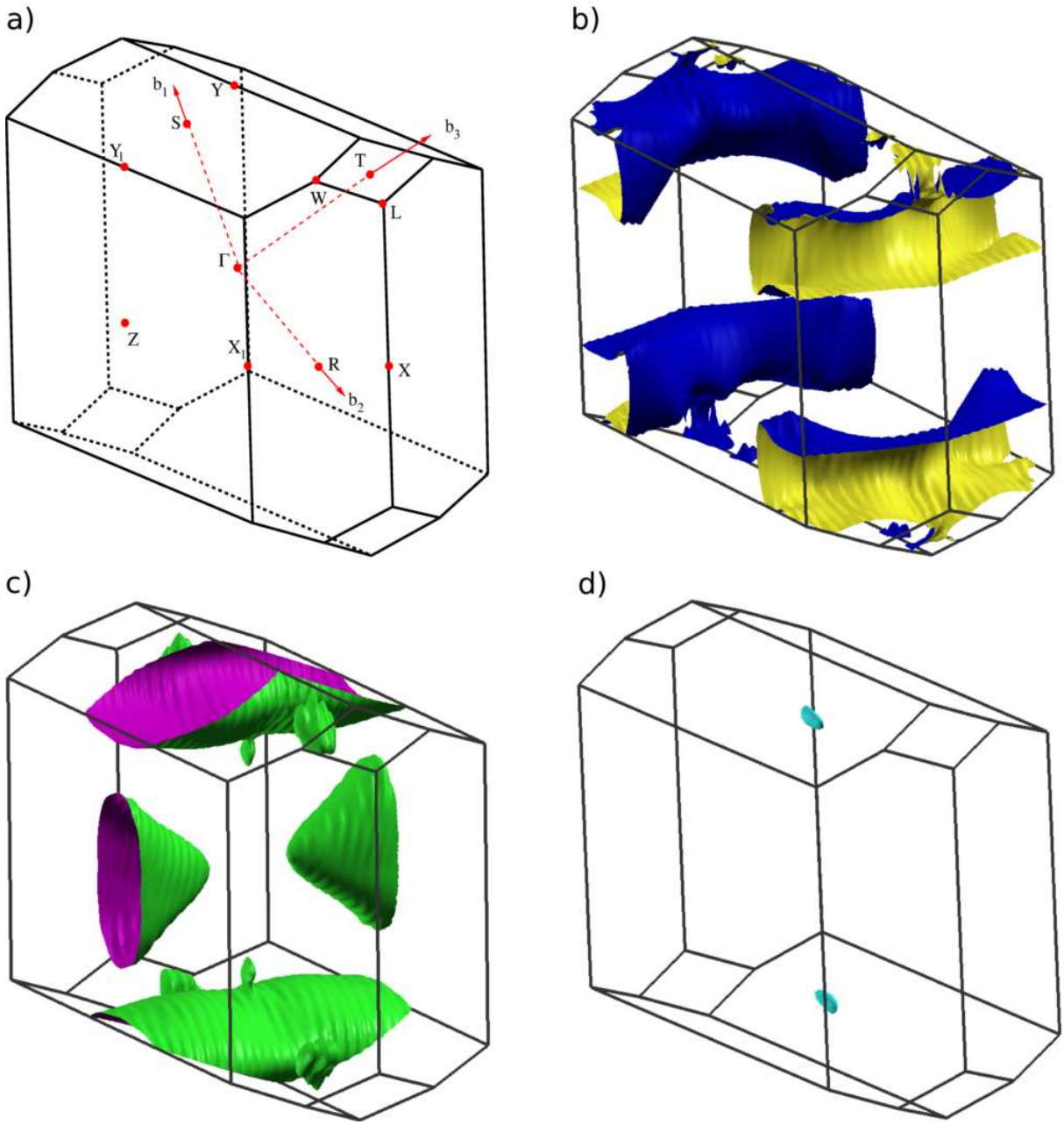

FIG. 3: The Brillouin (a) and the calculated Fermi surface sheets ((b),(c),(d)) for the body-centered orthorhombic crystal structure of NbPS.

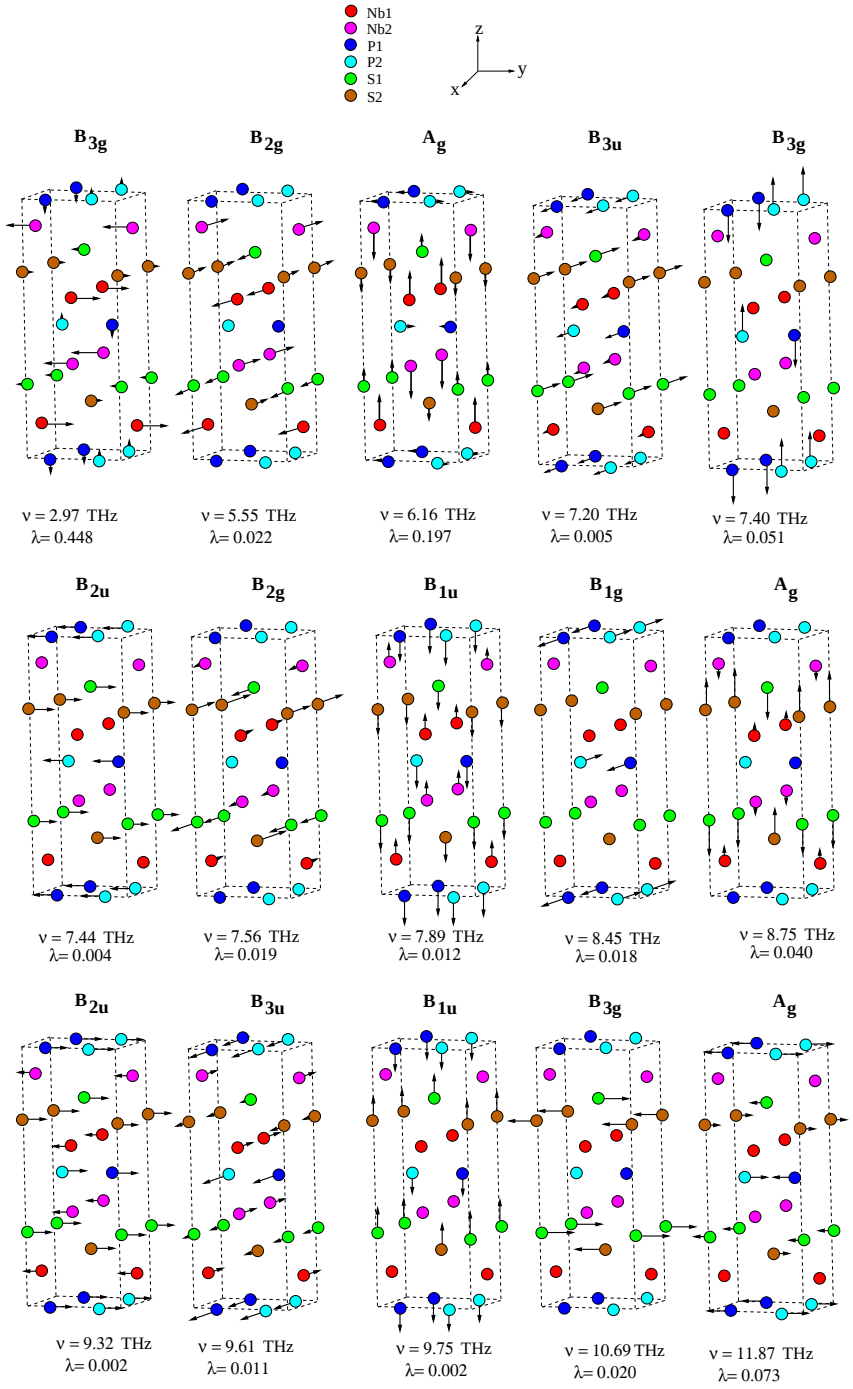

FIG. 4: The eigenvector representations, frequencies and electron-phonon coupling parameters of zone-center phonon modes for the NbPS superconductor.

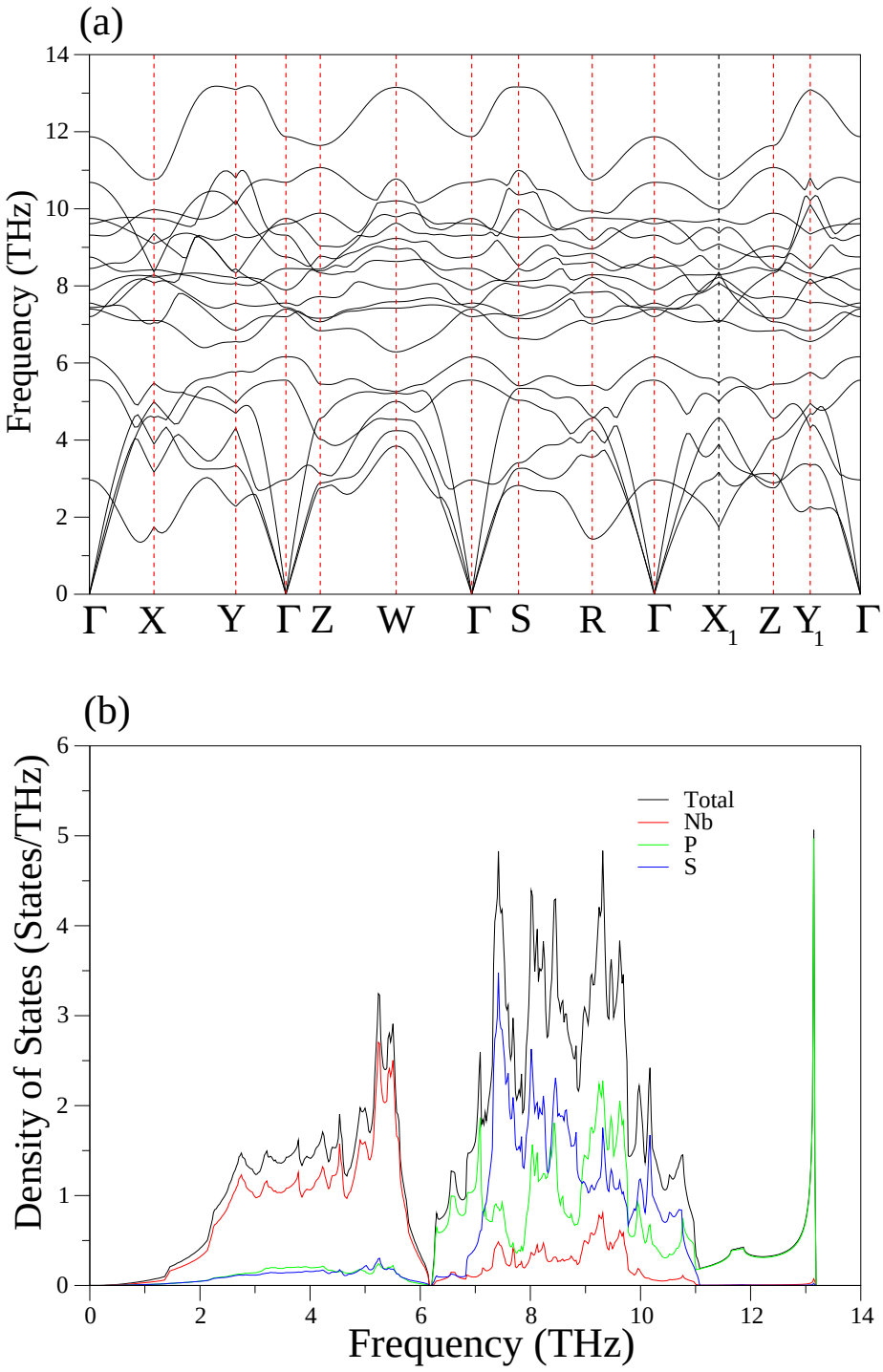

FIG. 5: (a) The calculated phonon spectrum of the NbPS superconductor plotted along the high symmetry directions of the body-centered orthorhombic Brillouin zone. (b) The calculated total and partial phonon density of states of NbPS.

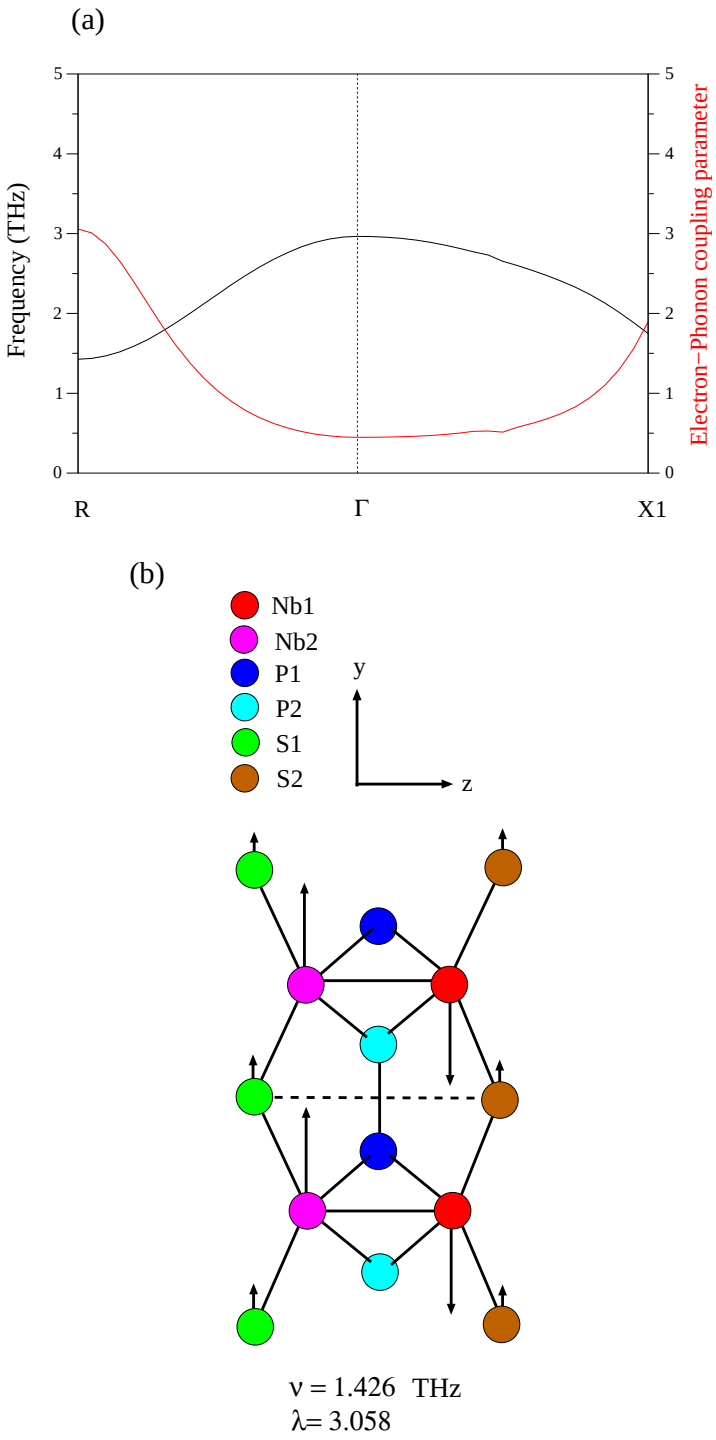

FIG. 6: (a) The frequency (black line) and electron-phonon coupling parameter (red line) of the lowest optical phonon mode along the R-Γ-X_1 symmetry direction in NbPS. (b) The eigenvector representation of the lowest optical phonon mode at the R symmetry point.

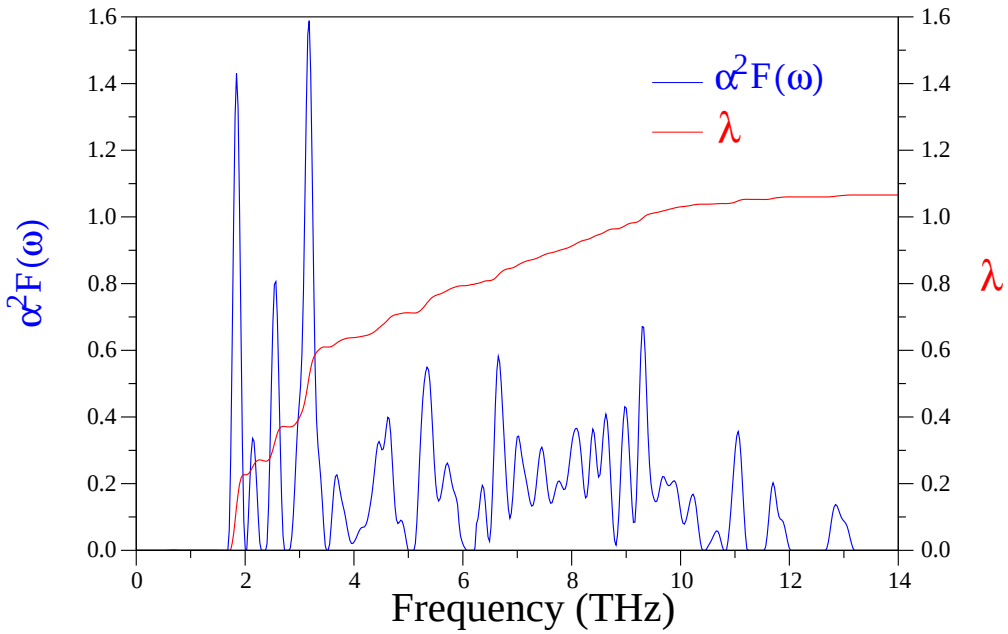

FIG. 7: The Eliashberg spectral function (blue line) and the frequency dependence of average electron-phonon coupling (red line) for the NbPS superconductor.